CD4(+) and CD8(+) cytotoxic Tlymphocytes may induce mesenchymal cell apoptosis in IgG(4)-related disease

Perugino, C.A.; Kaneko, N.; Maehara, T.; Mattoo, H.; Kers, J.; Allard-Chamard, H.; ... ; Pillai, S.

CD4$^+$ and CD8$^+$ cytotoxic T lymphocytes may induce mesenchymal cell apoptosis in IgG$_4$-related disease

Cory A. Perugino, DO,[a,b]* Naoki Kaneko, DDS, PhD,[a,c]* Takashi Maehara, DDS, PhD,[a,c]* Hamid Mattoo, PhD,[a,d] Jesper Kers, MD, PhD,[a,e,f] Hugues Allard-Chamard, MD, PhD,[a,g] Vinay S. Mahajan, MBBS, PhD,[a,h] Hang Liu, MD,[a,i] Emanuel Della-Torre, MD,[a,j] Samuel J. H. Murphy, BS,[a] Musie Ghebremichael, PhD,[a] Zachary S. Wallace, MD, MSc,[b] Marcy B. Bolster, MD,[b] Liam M. Harvey, BS,[b] Geetha Mylvaganam, PhD,[a] Yesim Tuncay, BS,[a] Lloyd Liang, BA,[k] Sydney B. Montesi, MD,[k] Xiuwei Zhang, PhD,[l] Akira Tinju, DDS,[c] Keita Mochizuki, DDS,[c] Ryusuke Munemura, DDS,[c] Mizuki Sakamoto, DDS, PhD,[c] Masafumi Moriyama, DDS, PhD,[c] Seiji Nakamura, DDS, PhD,[c] Nir Yosef, PhD,[l] John H. Stone, MD, MPH,[b] and Shiv Pillai, MBBS, PhD[a] *Cambridge and Boston, Mass; Fukuoka, Japan; Amsterdam, The Netherlands; Sherbrooke, Québec, Canada; Shenyang, China; Berkeley, Calif; and Milan, Italy*

GRAPHICAL ABSTRACT

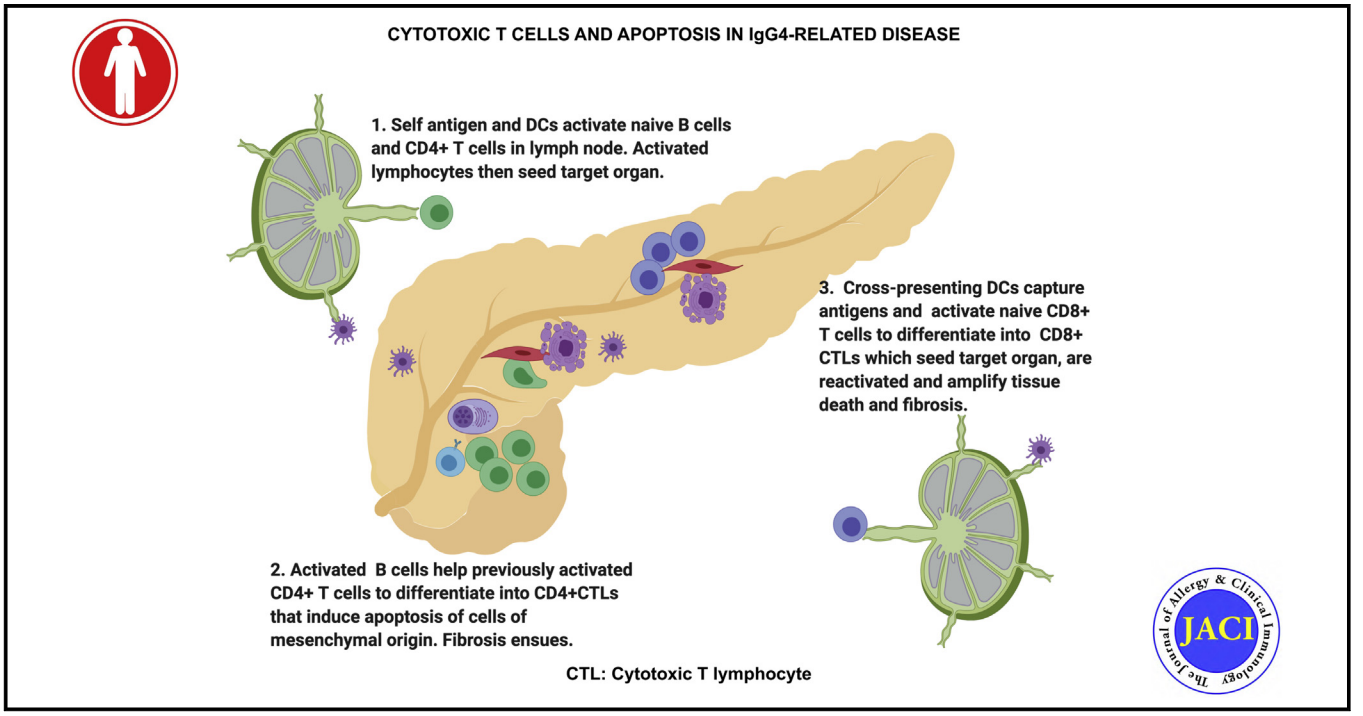

From [a]the Ragon Institute of MGH, MIT, and Harvard, Cambridge; [b]Division of Rheumatology, Allergy and Immunology, Massachusetts General Hospital, Boston; [c]the Section of Oral and Maxillofacial Oncology, Division of Maxillofacial Diagnostic and Surgical Sciences, Faculty of Dental Science, Kyushu University, Fukuoka; [d]the Immunology and Inflammation Therapeutic Area, Sanofi, Cambridge; [e]the Amsterdam UMC, University of Amsterdam, Amsterdam Infection & Immunity Institute (AI&II), Amsterdam Cardiovascular Sciences (ACS), Amsterdam; [f]the Van't Hoff Institute for Molecular Sciences (HIMS), University of Amsterdam, Amsterdam; [g]the Division of Rheumatology, Faculté de médecine et des sciences de la santé de l' Université de Sherbrooke et Centre de Recherche Clinique Étienne-Le Bel, Sherbrooke; [h]the Department of Pathology, Brigham and Women's Hospital, Boston; [i]the Department of Rheumatology and Immunology, First Hospital of China Medical University, Shenyang; [j]the Unit of Immunology, Rheumatology, Allergy, and Rare Diseases (UnIRAR), IRCCS San Raffaele Scientific Institute, Milan; [k]the Division of Pulmonary & Critical Care Medicine, Massachusetts General Hospital, Boston; and [l]the University of California, Berkeley.

*These authors contributed equally to this work.

This work was supported by the National Institutes of Health (NIH) Autoimmune Centers of Excellence (grant no. U19 AI 110495 to S.P.). C.A.P. was supported by a Rheumatology Research Foundation Scientist Development Award, a Scleroderma Foundation New Investigator Grant and a Sponsored Research Agreement with UCB. T.M. was supported by Japan Society for the Promotioin of Science (grant no. JP18KK0260) and the Takeda Science Foundation. J.K. was supported by a Work Visit Grant of the Amsterdam Infection and Immunity Institute. V.S.M. was supported by the NIH (grant no. AI113163). M.G. was supported by the National Institute of Allergy and Infectious Diseases (grant no. P30AI060354). E.D.-T. was supported by the Giovani Ricercatori Research Grant from the Cariplo Foundation. S.B.M. was supported by a Parker B. Francis Fellowship and a Scleroderma Foundation New Investigator Grant, and J.H.S. was supported by the NIH Autoimmune Centers of Excellence (grant no. UM1 AI1144295).

Disclosure of potential conflict of interest: The authors declare that they have no relevant conflicts of interest.

Received for publication February 13, 2020; revised May 8, 2020; accepted for publication May 18, 2020.

Available online May 30, 2020.

Corresponding author: Shiv Pillai, MBBS, PhD, Ragon Institute of MGH, MIT and Harvard, 400 Technology Square, Cambridge, MA 02139. E-mail: pillai@helix.mgh.harvard.edu.

0091-6749/$36.00

https://doi.org/10.1016/j.jaci.2020.05.022

Background: IgG_4-related disease (IgG_4-RD) is an immune-mediated fibrotic disorder that has been linked to $CD4^+$ cytotoxic T lymphocytes ($CD4^+$CTLs). The effector phenotype of $CD4^+$CTLs and the relevance of both $CD8^+$ cytotoxic T lymphocytes ($CD8^+$CTLs) and apoptotic cell death remain undefined in IgG_4-RD.

Objective: We sought to define $CD4^+$CTL heterogeneity, characterize the $CD8^+$CTL response in the blood and in lesions, and determine whether enhanced apoptosis may contribute to the pathogenesis of IgG_4-RD.

Methods: Blood analyses were undertaken using flow cytometry, cell sorting, transcriptomic analyses at the population and single-cell levels, and next-generation sequencing for the TCR repertoire. Tissues were interrogated using multicolor immunofluorescence. Results were correlated with clinical data.

Results: We establish that among circulating $CD4^+$CTLs in IgG_4-RD, $CD27^{lo}CD28^{lo}CD57^{hi}$ cells are the dominant effector subset, exhibit marked clonal expansion, and differentially express genes relevant to cytotoxicity, activation, and enhanced metabolism. We also observed prominent infiltration of granzyme A–expressing $CD8^+$CTLs in disease tissues and clonal expansion in the blood of effector/memory $CD8^+$ T cells with an activated and cytotoxic phenotype. Tissue studies revealed an abundance of cells undergoing apoptotic cell death disproportionately involving nonimmune, nonendothelial cells of mesenchymal origin. Apoptotic cells showed significant upregulation of HLA-DR.

Conclusions: $CD4^+$CTLs and $CD8^+$CTLs may induce apoptotic cell death in tissues of patients with IgG_4-RD with preferential targeting of nonendothelial, nonimmune cells of mesenchymal origin. (J Allergy Clin Immunol 2021;147:368-82.)

Key words: *IgG_4-RD, $CD4^+$CTL, $CD8^+$CTL, apoptosis, $CD28^{lo}$, CD28(null)*

IgG_4-related disease (IgG_4-RD) is an insidiously progressive condition associated with chronic antigen-driven immune activation resulting in fibrosis.[1,2] This disease affects many organ systems and is characterized by tumor-like inflammatory masses composed of T cells enmeshed in an expanded fibrotic stroma with activated B cells and antibody-secreting cells that predominantly express IgG_4.[3,4] B cells are of clear pathogenic importance as evidenced by the efficacy of B-cell depletion[5] and may even play a direct profibrotic role.[6] However, T cells dominate the cellular infiltrate of affected tissues.[7]

Most studies on the contribution of T cells to the pathogenesis of IgG_4-RD have focused on the $CD4^+$ T- cell compartment and $CD4^+$ cytotoxic T lymphocytes ($CD4^+$CTLs) have been identified as the dominant tissue-infiltrating $CD4^+$ T-cell subset.[8-10] In IgG_4-RD, $CD4^+$CTLs are clonally expanded in the blood, accumulate at lesional sites in high numbers, are functionally cytotoxic, and secrete profibrotic factors.[8,9] Moreover, $CD4^+$CTLs have been shown to decline in numbers in response to B-cell depletion therapy, an observation that may be explained by the potential for activated B-cell subsets to present antigen to tissue-infiltrating $CD4^+$CTLs.[8,10] The heterogeneity of $CD4^+$CTLs, including the identification of both effector and precursor subsets, has been reported in the context of prior dengue viral infection[11] but has not yet been explored in IgG_4-RD or any other chronic inflammatory disease. Similarly, $CD4^+$ T cells that are phenotypically consistent with $CD4^+$CTLs have been described in the setting of multiple other autoimmune diseases[12-17] but how these cells compare with those observed in IgG_4-RD is unknown. In contrast, the $CD8^+$ T-cell compartment has only been interrogated in a limited way in this disease.[18]

Apoptotic cell death has been invoked as a prelude to fibrosis in various conditions including idiopathic pulmonary fibrosis and systemic sclerosis.[19,20] We have recently identified $CD4^+$CTLs and more specifically, endothelial cell apoptosis, as potential contributing factors to the pathogenesis of systemic sclerosis.[21] However, similar *in situ* evidence of cytotoxicity has not yet been explored in tissues affected by IgG_4-RD. Here, using blood and tissue samples from patients with IgG_4-RD, we have defined an effector subset of $CD4^+$CTLs, explored the relevance of $CD8^+$ T cells in this condition, and performed studies that suggest that apoptotic cell death may be of mechanistic relevance in IgG_4-RD.

Abbreviations used

$CD4^+$CTL:	$CD4^+$ cytotoxic T lymphocyte
$CD8^+$CTL:	$CD8^+$ cytotoxic T lymphocyte
FDR:	False-discovery rate
GZMA:	Granzyme A
GZMB:	Granzyme B
IgG_4-RD:	IgG_4-related disease
PRF:	Perforin
T_{EM}:	T effector/memory
T_{EMRA}:	T Effector/memory RA expressing

METHODS

Patient cohorts

IgG_4-RD blood samples (n = 48) and age-matched healthy donors (n = 20) were obtained through the Massachusetts General Hospital Division of Rheumatology. IgG_4-RD was defined by either the fulfillment of established histopathologic diagnostic criteria or American College of Rheumatology (ACR)/European League Against Rheumatism (EULAR) IgG_4-RD Classification Criteria.[3,4] An IgG_4-RD Responder Index greater than or equal to 1 was considered active disease.[22] Eight of these patients were on some form of immunosuppression, whereas 41 were clinically active at the time of blood collection. Severe disease was defined by the presence of active disease involving the lung, aorta, bile duct, pancreas, kidney, or meninges, whereas diseases limited to the orbit, lacrimal glands, salivary glands, sinuses, or retroperitoneum were considered mild. Healthy donors were defined by lacking any current history or history of malignancy, autoimmune disease, or recurrent/chronic infections. Subjects with sarcoidosis were recruited through the Massachusetts General Hospital Division of Pulmonary & Critical Care Medicine. Patients with sarcoidosis were diagnosed as previously described.[23] Specifically, patients with sarcoidosis were free of cross-sectional chest imaging, and pulmonary function testing for each subject with sarcoidosis was reviewed by a pulmonologist with expertise in fibrotic lung disease (S.B.M.) and only those without evidence of lung fibrosis were used for these studies. Clinical and demographic data on all subjects used for these studies are presented in Table E1 in this article's Online Repository at www.jacionline.org. PBMCs were isolated by Ficoll density gradient centrifugation within 4 hours of phlebotomy and preserved in gas-phase liquid nitrogen until the time of use. Data such as sex, age, treatment status, disease activity, clinical manifestations, and laboratory parameters were extracted from the medical records of all patients.

Submandibular glands from 21 patients with IgG_4-RD, labial salivary glands from 15 patients with Sjogren syndrome, and submandibular glands from 10 patients with chronic sialadenitis were obtained from the Department of Oral and Maxillofacial Surgery of Kyushu University Hospital, Fukuoka,

Japan. All these patients had been evaluated between 2008 and 2018 at the Kyushu University Hospital. Sjogren syndrome was diagnosed as previously defined.[24] Chronic sialadenitis is a nonspecific inflammatory disease of the salivary glands linked to sialolithiasis and was diagnosed on clinical grounds.

Flow cytometry

Frozen PBMCs were thawed and washed in complete Dulbecco modified Eagle medium. Before antibody staining, Fc receptors were blocked using Human TruStain FcX (BioLegend, San Diego, Calif, 422302) at a concentration of 1:20 on ice for 15 minutes. Cells were stained for 20 minutes on ice, protected from light, at a concentration of 20 million cells/mL using the following antibody panel (manufacturer, clone, concentration used): anti-human CD3-BUV395 (BD Biosciences, San Jose, Calif, Clone SK7, 1:40), anti-human CD57-PE (BD Biosciences, Clone NK-1, 1:400), anti-human CD8-BV785 (BioLegend, Clone SK1, 1:300), anti-human CD45RA-BV605 (BioLegend, Clone HI100, 1:300), CD4-BUV805 (BD Biosciences, Clone SK3, 1:80), anti-human CD28-BV480 (BD Biosciences, Clone CD28.2, 1:40), anti-human CCR7-APC/Cy7 (BioLegend, Clone G043H7, 1:20), and anti-human SLAMF7-A648 (BD Biosciences, Clone 235614, 1:10). Cells were washed with 1% BSA in PBS after staining, centrifuged, and resuspended in 1% BSA in PBS. Just before flow cytometry, dead cells were stained with SYTOX AADvanced Dead Cell Stain (Thermo Fisher Scientific, Waltham, Mass, S10274). The following antibodies were used for intracellular flow cytometry studies: antihuman granzyme A (GZMA)-PE/Cy7 (BioLegend, Clone CB9, 1:10), anti-human granzyme B (GZMB)-BV421 (BD Biosciences, Clone GB11, 1:25), anti-human GZMK-fluorescein isothiocyanate (BioLegend, Clone GM26E7, 1:25), and anti-human perforin (PRF)-BV711 (BioLegend, Clone dG9, 1:25). Anti-human CX3CR1-BV650 (BioLegend, Clone 2A9-1, 1:25) was also used for extracellular staining before intracellular staining. Cells were fixed and permeabilized using the fixation/permeabilization solution kit from BD Biosciences (catalog #554714) according to the manufacturer's protocol. Flow cytometry was performed on a BD LSR II (BD Biosciences), and rainbow tracking beads were used to ensure consistent signals between flow cytometry batches. FCS files were analyzed using FlowJo (Carrboro, NC) software (version 10).

Multicolor immunofluorescence staining

Tissue samples were fixed in formalin, embedded in paraffin, and sectioned. These specimens were incubated with antibodies: CD3 (clone: A045229-2; DAKO), CD4 (clone: CM153A; Biocare, Kuala Lumpur, Malaysia), CD19 (clone: CM310 A, B; Biocare), CD8 (clone: ab85792; Abcam, Cambridge, Mass), CD31 (clone: 3528; Cell Signaling Technology, Danvers, Mass), CD68 (clone: ab955; Abcam), cleaved caspase-3 (clone: 9664; Cell Signaling Technology), GZMA (clone: LS-C312742; LSBio, Seattle, Wash), CD28 (clone: ab243228; Abcam), CD45RA (clone: 158-4D3; Novus Biologicals, Littleton, Colo), vimentin (clone: 5741; Cell Signaling Technology), α-SMA (clone: 19245; Cell Signaling Technology), pan-CK (clone: ab27988; Abcam), AQP5 (clone: ab92320; Abcam), HLA-DR (clone: ab20181; Abcam), and SLAMF7 (clone: HPA055945; Sigma Aldrich, St Louis, Mo) followed by incubation with secondary antibody using an OpalTM Multiplex Kit (Perkin Elmer, Waltham, Mass). The samples were mounted with ProLong Diamond Antifade mountant containing 4'-6-diamidino-2-phenylindole, dihydrochloride (Thermo Fisher Scientific).

Microscopy and quantitative image analysis

Images of the tissue specimens were acquired using the TissueFAXS platform (TissueGnostics, Vienna, Austria). For quantitative analysis, the entire area of the tissue was acquired as digital grayscale images in 5 channels with filter settings for fluorescein isothiocyanate, Cy3, Cy5, and AF75 in addition to 4'-6-diamidino-2-phenylindole, dihydrochloride. Cells of a given phenotype were identified and quantitated using the TissueQuest software (TissueGnostics), with cutoff values determined relative to the positive controls. For tissue staining, 4'-6-diamidino-2-phenylindole, dihydrochloride was used to define nucleated cells along with the following markers to define each respective cell type: T cells ($CD3^+$), B cells ($CD19^+$), macrophage ($CD68^+$), endothelial cell ($CD31^+$), acinar cell ($AQP5^+$, $PanCK^+$), ductal cell $AQP5^-$, $PanCK^+$), myoepithelial cell ($vimentin^+$, $\alpha\text{-}SMA^+$), mesenchymal cell ($vimentin^+$, $\alpha\text{-}SMA^-$, $CD19^-$, $CD3^-$), $CD4^+$CTLs ($CD4^+$, $GZMA^+$), and $CD8^+$ cytotoxic T lymphocytes ($CD8^+$CTLs) ($CD8^+$, $GZMA^+$). In Fig 5, *E*, to quantify the relative contributions of each cell type to overall apoptotic cell death, we excluded $CD3^+$ T cells from the analysis due to the confounding influence of activation-induced cell death. This microscopy-based multicolor tissue cytometry software permits multicolor analysis of single cells within tissue sections similar to flow cytometry. The principle of the method and the algorithms used have been described in detail elsewhere.[25]

FACS-sorting, RNA sequencing, and TCR repertoire studies

Frozen PBMCs were thawed, washed, and stained with the same antibody panel as used for flow cytometry experiments, above. Consistent with our flow cytometry studies, effector $CD4^+$CTLs were sorted on the basis of the following gates: $CD3^+$ $CD4^+$ $CD8^-$ $CCR7^-$ $CD45RA^-$ $SLAMF7^+$ $CD28^{lo}$ $CD57^{hi}$. $CD4^+$ naive T cells were sorted on the basis of the following gates: $CD3^+$ $CD4^+$ $CD8^-$ $CCR7^+$ $CD45RA^+$. Cells were sorted directly into 350 μL RLT-BME lysis buffer, vortexed briefly, and immediately frozen on dry ice. Cells were sorted on a FACSAria II with FACSDiva version 7. RNA was isolated from sorted cell lysates using RNeasy Plus Micro Kits (Qiagen, 74034). For bulk RNA sequencing, isolated RNA was immediately processed through RT-PCR, as previously described.[26] For single-cell RNA sequencing, cells were FACS-sorted into lysis buffer of a 96-well plate format and processed as previously described.[27] For bulk RNA sequencing analysis of effector/memory $CD8^+$ T cells, a technical replicate from a subject with IgG_4-RD was available and included in the analysis. For TCR repertoire, isolated RNA was immediately processed through 5'RACE RT-PCR, as previously described.[28] For gene-specific amplification of the TCRβ gene, the following reverse primer was used: 5′ TGCTTCTGATGGCTCAAACA CAGCGACCT 3′.

Statistical analysis

GraphPad Prism version 8 was used for statistical analysis, curve fitting, and linear regression. A 2-tailed Mann-Whitney *U* test was used to calculate *P* values for continuous, nonparametric variables. For categorical variables, Fisher exact test was used to calculate *P* values. For comparing more than 1 population, Kruskal-Wallis testing was used with Dunn's multiple comparison testing. Pearson correlation coefficient was used to quantify the strength of linear relationship between variables. A *P* value of less than .05 was considered significant.

Bulk RNA sequencing. Raw FASTA files (read 1 and read 2) were processed with the zUMIs v2.2 pipeline using the splice-aware aligner STAR v2.5.4a, SAMtools v1.9, and pigz v2.3.4(61). In short, reads were filtered according to a predefined list matching the custom-made well barcodes in the oligo-dTs and unique molecular identifiers were then collapsed. The remaining reads were mapped to the reference genome with use of the STAR aligner. Exon counts from mapped reads were imported into R studio v1.1.456 and further processed for statistical analysis with DESeq2 v1.22.1. Because we compare multiple cellular subtypes per patient, we controlled for between-patient variability in the design matrix. Fitting of the models' dispersion to the mean intensity was performed with local regression, and the effect sizes were calculated with the postcounts estimator in DESeq. Dispersion plot fits were visually validated for goodness-of-fit. We performed pairwise comparison between cell subtypes of interest, and the per-gene *P* values were adjusted for multiple testing by Benjamini Hochberg false-discovery rate (FDR). Gene-set enrichment analysis was done with the GSEABase package v1.44.0 (fgsea algorithm) with 10,000 permutations, gene-set size between 5 and 2000, and a Benjamini Hochberg-FDR–adjusted *P* value cutoff of 0.25. Gene-set lists were downloaded from the MSigDB v6.2 at the Broad Institute of MIT & Harvard and included gene sets from the GO, KEGG, BioCarta, Reactome, and Hallmark databases. Custom gene sets

were created by extraction of the cell-type–specific gene expression signatures from Stanford's CIBERSORT tool and previous studies describing gene expression signatures on $CD4^+$CTLs.[8,11,29]

T-cell receptor repertoire analysis. Processed files were imported in VDJtools v1.1.4 for statistical analysis. Basic V-J usage per cell type was analyzed by computing read frequencies. Clonotype abundances were calculated by CDR3 nucleotide, V and J matching among $CD4^+$ CTLs.

Study approval

These studies were approved by the institutional review boards at the Massachusetts General Hospital, University of Michigan Medical Center, Hospital of the University of Pennsylvania, and Kyushu University Hospital. All patients provided written informed consent before inclusion in the study.

RESULTS

An effector subset of $CD4^+$CTLs is characterized by the loss of surface CD28 and a gain of CD57 expression

Previously, we identified SLAMF7 as a surface marker capable of distinguishing $CD4^+$CTLs.[8] These earlier studies relied on the loss of CD27 in defining effector/memory $CD4^+$ T cells. However, downregulation of CD27 and the generation of $CD4^+$CTLs are both linked with chronic antigen exposure and therefore, the $CD27^{lo}$ $CD4^+$ T-cell compartment may be biased toward higher $CD4^+$CTL numbers relative to other $CD4^+$ T-cell subsets that are more acutely induced. We explored the heterogeneity of $CD4^+$CTLs by flow cytometry and first isolated the downstream effect of CD27 downregulation by comparing alternative gating strategies to define effector/memory T (T_{EM}) cells. In fact, we observed more than a 2-fold enrichment of $CD4^+SLAMF7^+$ T cells by pregating on $CD27^{lo}$ $CD4^+$ T_{EM} cells (see Fig E1 in this article's Online Repository at www.jacionline.org). Thereafter, relying on the dual loss of CCR7 and CD45RA to define $CD4^+$ T_{EM} cells, we examined $CD4^+SLAMF7^+$ T_{EM} cells by flow cytometric tSNE analysis and identified 3 subsets with clustering determined by the gain or loss of CD28 and/or CD57 (Fig 1, *A*). Within these subsets, the expression or downregulation of CD27 correlated with the expression pattern of CD28. The corresponding flow cytometry plot of $CD4^+SLAMF7^+$ T_{EM}-cell subsets is presented in Fig 1, *B*. Among these subsets, the $CD28^{lo}CD57^{hi}$ cells demonstrated the greatest enrichment for cytotoxic proteins including GZMA, GZMB, and PRF, as well as markers associated with a $CD4^+$CTL effector phenotype including $CX3CR1^+$ and $CD127^{lo}$.[11,30] $CD28^{lo}CD57^{hi}$ $CD4^+SLAMF7^+$ T_{EM} cells shared a phenotype most analogous to bone fide $CD8^+$ cytotoxic effector T cells (Fig 1, *C*). Many of the markers studied showed a gradation of expression across $CD4^+SLAMF7^+$ T_{EM}-cell subsets, suggesting a continuum of differentiation states ranging from $CD28^{hi}CD57^{lo}$ "precursor" cells, to $CD28^{lo}CD57^{lo}$ "intermediate" cells, to $CD28^{lo}CD57^{hi}$ "effector" cells (Fig 1, *D*; see Fig E2 in this article's Online Repository at www.jacionline.org). Molecular characterization of $CD4^+SLAMF7^+$ T_{EM} cells by single-cell RNA sequencing and Monocle analysis was consistent with this developmental trajectory (Fig 1, *D*).

By TCR sequencing, we observed clonal connectivity between $CD4^+SLAMF7^+$ T_{EM}-cell subsets, with the greatest overlap between effector and intermediate cells (Fig 2, *A*). Striking clonal expansion was also observed such that the top 10 clones consumed the vast majority of TCR sequence reads among these subsets (Fig 2, *B*). The degree of clonal expansion among precursor $CD4^+SLAMF7^+$ T_{EM} cells was contingent on how connected the repertoire was to those of the intermediate and effector subsets (Fig 2, *A* and *B*; see Fig E3 in this article's Online Repository at www.jacionline.org).

In contrast to healthy donors, in whom the precursor subset consistently dominated, the $CD4^+SLAMF7^+$ T_{EM} compartment from patients with IgG_4-RD was predominantly of the effector or intermediate phenotype (Fig 2, *C*; see Fig E4, *A*, in this article's Online Repository at www.jacionline.org). Although the intermediate phenotype among $CD4^+SLAMF7^+$ T_{EM} cells was expanded in some patients with IgG_4-RD and rarely present in significant numbers in controls, it constituted only 10% to 15% of all $CD4^+SLAMF7^+$ T_{EM} cells (Fig E4, *B*). The gating strategy used for these studies is presented in Fig E5 in this article's Online Repository at www.jacionline.org. In addition to the prominent clonal expansion and accumulation of effector $CD4^+SLAMF7^+$ T_{EM} cells, this subset correlated with multiple clinical parameters reflective of disease severity in IgG_4-RD (Fig 2, *D*). In contrast, the more limited clinical phenotype confined to the glandular tissues of the head and neck was inversely associated with effector $CD4^+$CTL expansion. Additional immunophenotyping revealed that large proportions of effector $CD4^+$CTLs coexpress the adhesion molecule GPR56, the activation markers HLA-DR and PD-1, and the chemokine receptor CXCR3, as described among $CD4^+$CTLs in the contexts of antiviral responses, systemic lupus erythematosus, and rheumatoid arthritis (see Fig E6 in this article's Online Repository at www.jacionline.org).[12,31,32]

Taken together, these data define $CD4^+$ T_{EM} cells that have gained surface expression of SLAMF7 and CD57 but lost the costimulatory molecules CD27 and CD28 as a circulating effector subset of $CD4^+$CTLs of potential pathogenic relevance in the setting of chronic inflammation.

Effector $CD4^+$CTLs demonstrate a gene signature of activation and accumulate in lesional tissues

We isolated circulating effector $CD4^+$CTLs from patients with IgG_4-RD and performed RNA sequencing. Compared with naive $CD4^+$ T cells from the same subjects, we identified 7392 differentially expressed transcripts, with more than half being upregulated by $CD4^+$CTLs (Fig 3, *A*). Mapping of potential protein-protein interactions yielded a highly interactive network greatly enriched by genes related to cytotoxicity (FDR, 2.09×10^{-11}), cell activation (FDR, 3.08×10^{-7}), and cell migration (FDR, 0.0102) (Fig 3, *B*). Genes relevant to each biologic process include *GZMA*, *GZMB*, *GZMM*, *GNLY*, *PRF1*, *CX3CR1*, and *NKG7* related to cytotoxicity, *CD40LG*, *DOCK2*, *SLAMF7*, and *PIK3R5* related to lymphocyte activation, and *ITGAL*, *ITGAM*, *NFATC2*, *GPR56*, and *TGFBR3* related to cell-matrix interactions. By gene-set enrichment analysis, we additionally observed upregulation of collections of cytokines (*CCL4*, *CCL5*, *IL1B*, *IFNG*), cytokine receptors (*PTGDR*, *IL18R1*), and chemokine receptors (*CCR5*, *CXCR6*) that may be relevant to the role of effector $CD4^+$CTLs in orchestrating a chronic inflammatory immune response and in homing to inflamed tissues (Fig 3, *C*). Moreover, the transcriptome of effector $CD4^+$CTLs was enriched for gene sets related to increased cellular metabolism including those of oxidative phosphorylation, fatty acid metabolism, mTORC1 signaling,

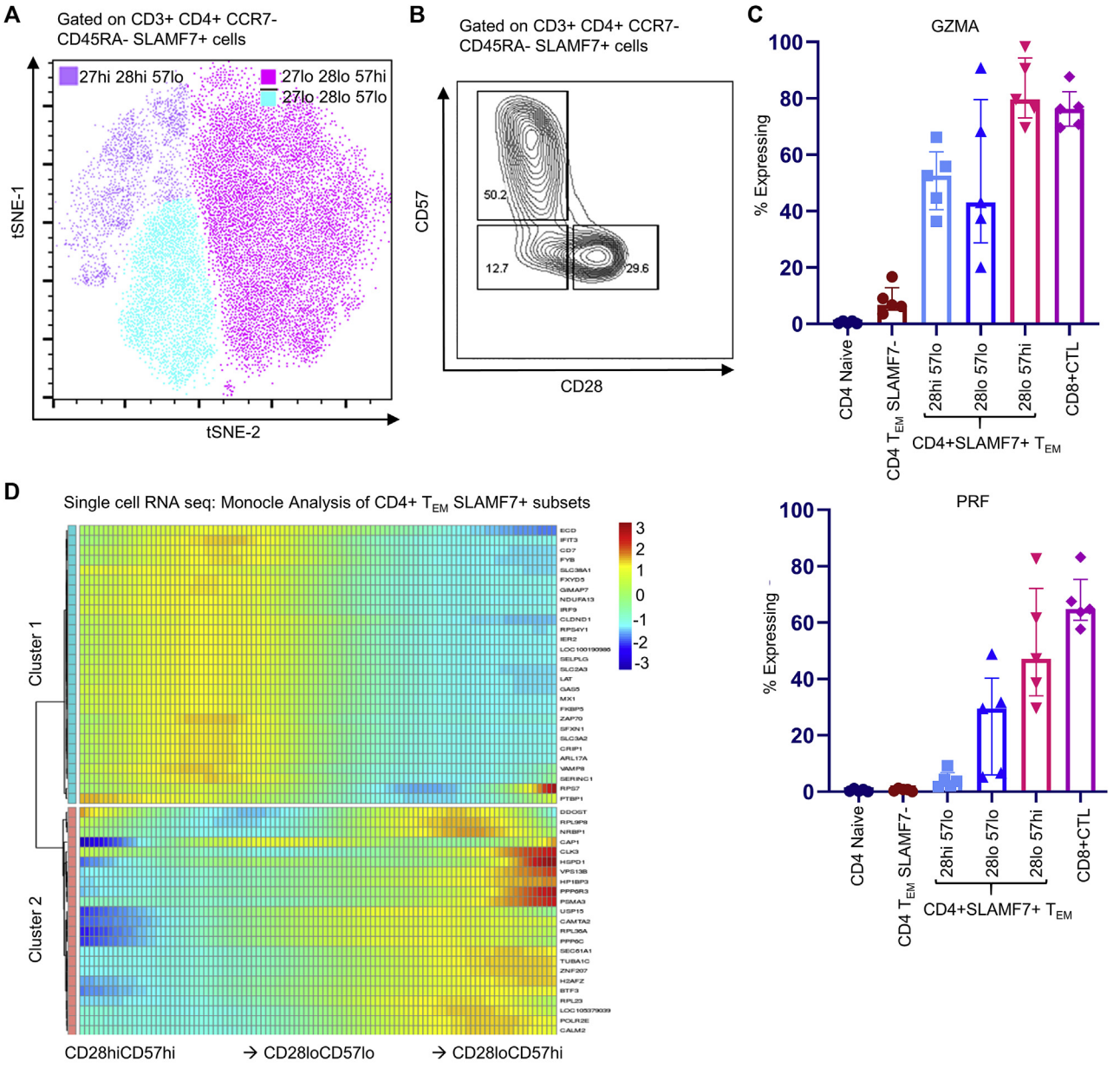

FIG 1. $CD27^{lo}$ $CD28^{lo}$ $CD57^{hi}$ defines an effector subset of $CD4^+$CTLs. **A,** tSNE analysis reveals heterogeneity within the $CD4^+$ $CCR7^{lo}$ $CD45RA^{lo}$ $SLAMF7^+$ population from the blood of a representative patient with IgG_4-RD. **B,** Representative flow contour plot displaying distinct subsets of $SLAMF7^+$ $CD4^+$ T_{EM} cells in the blood of a representative patient with IgG_4-RD. **C,** Intracellular flow cytometry for GZMA and PRF showing the greatest frequency of cytotoxic protein expression among $CD28^{lo}CD57^{hi}$ $CD4^+SLAMF7^+$ T cells compared with other subsets. $CCR7^-$ $CD45RA^+$ $CD28^{lo}CD57^{hi}$ $CD8^+$ $SLAMF7^+$ T cells were used to represent $CD8^+$CTLs. Displayed are medians (bars) and interquartile range (error bars). **D,** Monocle analysis of single-cell sequencing data of $SLAMF7^+$ $CD4^+$ T_{EM}-cell subsets suggesting a differentiation trajectory.

and cholesterol homeostasis (see Fig E7 in this article's Online Repository at www.jacionline.org).

We previously demonstrated the marked accumulation of $CD4^+$CTLs within IgG_4-RD lesions.[8] To examine the activation state of tissue-infiltrating $CD4^+$CTLs, we quantified the relative contribution of $CD28^{lo}$ and $CD28^{hi}$ $CD4^+$CTLs in lesional tissues (Fig 3, *D*). $CD4^+$CTLs of both differentiation states were identified within tissues with an overall comparable contribution (Fig 3, *E*).

$CD8^+$CTLs accumulate in tissues affected by IgG_4-RD in comparable numbers to $CD4^+$CTLs

Although multiple reports have linked $CD4^+$CTLs to human IgG_4-RD, HLA class I–restricted $CD8^+$CTL responses have also been suggested to have a pathogenic role in what has been described as a mouse model of this disease, though the disease process in this model affects pancreatic islets and more closely mimics existing models of type I diabetes.[33] We explored the possibility that activated $CD8^+$CTLs may contribute to the

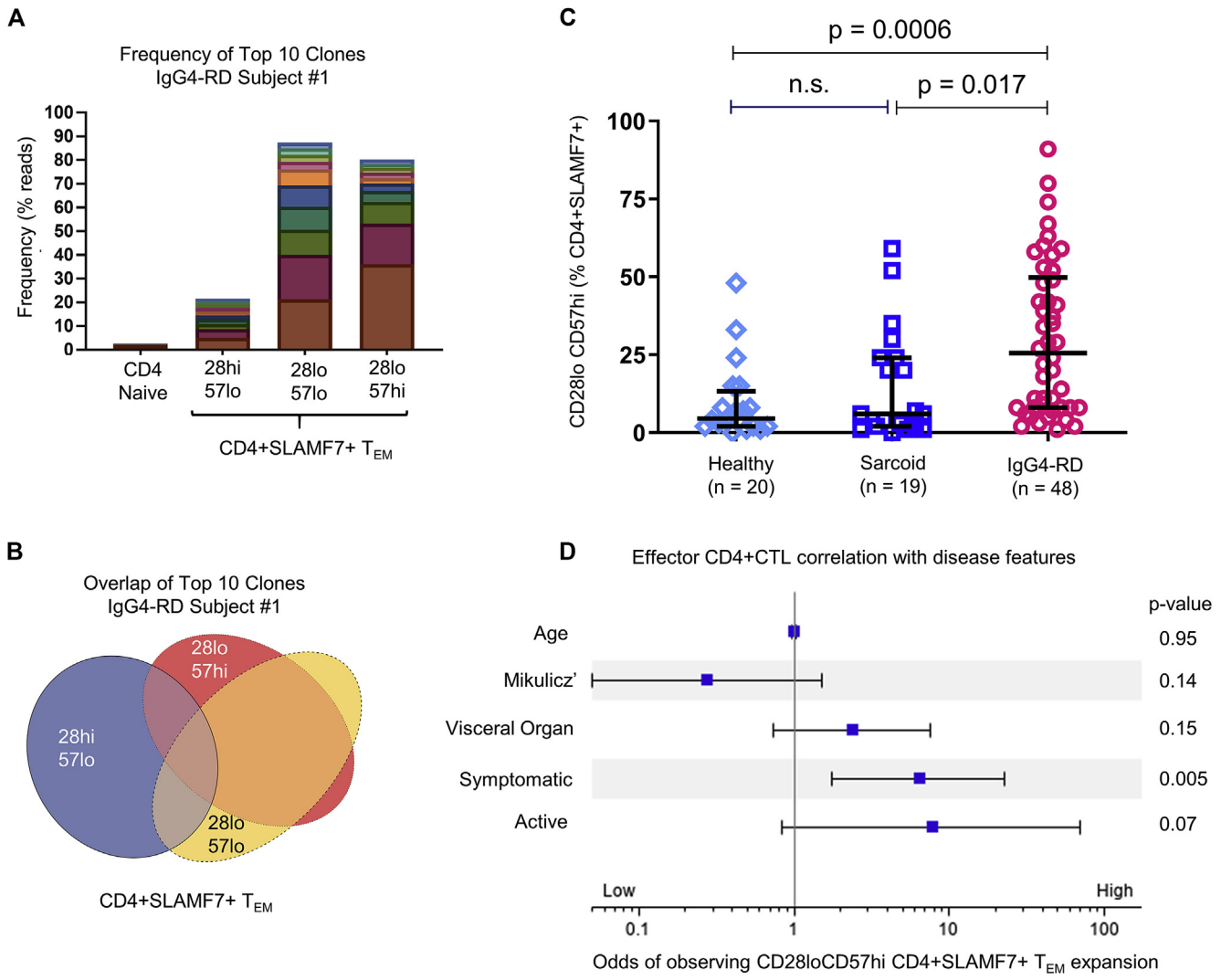

FIG 2. $CD28^{lo}$ $CD57^{hi}$ $CD4^{+}$CTLs are clonally expanded in IgG_4-RD and correlate with a more severe clinical phenotype. **A,** Stacked bar chart displays the frequency of the top 10 clones within each $CD4^{+}$CTL subset. $CD28^{lo}$ subsets show marked clonal expansion, with the top clones dominating the repertoire. **B,** Venn diagram showing % overlap of top 10 clones from each $CD4^{+}SLAMF7^{+}$ T-cell subset, with the greatest overlap observed between the $CD28^{lo}$ subsets. **C,** Dot plot of flow cytometry data displaying significant accumulation of $CD28^{lo}CD57^{hi}$ $CD4^{+}$ $SLAMF7^{+}$ T cells in the blood of patients with IgG_4-RD (n = 48) compared with nonfibrotic sarcoidosis (n = 19) and age-matched healthy donors (n = 20). Bars represent medians and interquartile ranges. *P* values calculated by ANOVA, with Kruskal-Wallis test to control for multiple comparisons. **D,** Forrest plot displaying the odds of observing an expanded $CD28^{lo}CD57^{hi}$ $SLAMF7^{+}$ $CD4^{+}$ T_{EM}-cell population in the blood based on clinical parameters of disease severity. *P* values calculated by logistic regression and are unadjusted for multiple comparisons. *n.s.*, Nonsignificant.

$CD4^{+}$CTL-dominated T-cell infiltrate that we previously described in IgG_4-RD. In quantitative analyses, we observed $CD4^{+}$ T cells in greater numbers than $CD8^{+}$ T cells in lesions, but both cell types infiltrated affected tissues in high numbers, with approximately 2000 $CD4^{+}$ and 1500 $CD8^{+}$ T cells being identified per mm^2, on average (Fig 4, *A* and *B*). However, using GZMA as a surrogate marker of cytotoxic capacity, we observed similar absolute numbers of $CD4^{+}$CTLs and $CD8^{+}$CTLs infiltrating tissues affected by IgG_4-RD (Fig 4, *C*). Exploring the tissue-infiltrating $CD8^{+}$CTLs further, we found that the vast majority had an activated phenotype with the loss of surface expression of the costimulatory receptor, CD28 (Fig 4, *D* and *E*).

A subset of $CD8^{+}$CTLs is activated, clonally expanded, and uses unique TCR Vβ genes in IgG_4-RD

We studied circulating $CD8^{+}$ T-cell subsets from patients with IgG_4-RD. An established phenotype of highly antigen-exposed $CD8^{+}$ T cells includes features of heightened cytotoxic capacity, the loss of CD28 expression, and the gain of CD57 expression.[34,35] Consistent with a highly cytotoxic phenotype, the vast majority of $CD28^{lo}CD57^{hi}$ $CD8^{+}$ T cells in the blood of patients with IgG_4-RD expressed GZMA and PRF (Fig 1, *C*) and to a lesser extent, GZMB (Fig E2). We observed a marked expansion of $CD28^{lo}CD57^{hi}$ $CD8^{+}$CTLs in patients with more severe IgG_4-RD compared with patients with a mild clinical phenotype

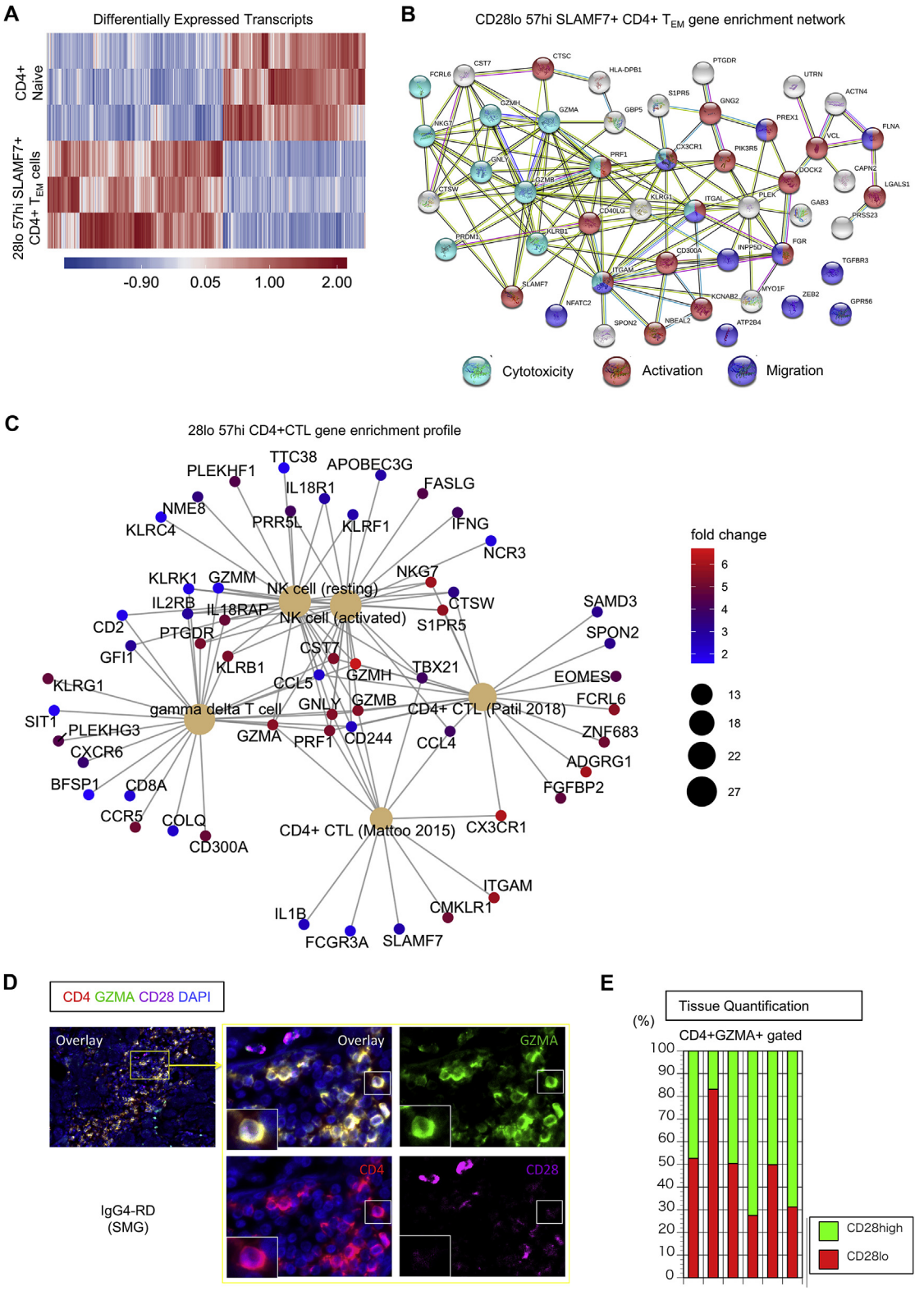

FIG 3. CD28^{lo} CD57^{hi} CD4^{+}CTLs display gene signatures of cytotoxicity, activation, and tissue migration. **A,** Heat map displaying 7392 differentially expressed transcripts between CD28^{lo}CD57^{hi} SLAMF7^{+} CD4^{+} T_{EM} cells and CD4^{+} naive T cells. **B,** STRING analysis representing predicted protein-protein interactions among upregulated genes by CD28^{lo} CD57^{hi} SLAMF7^{+} CD4^{+} T_{EM} cells. Number of lines connecting each node represents the degree of evidence for interaction. **C,** CNET plot showing genes enriched for by CD28^{lo} CD57^{hi} SLAMF7^{+} CD4^{+} T_{EM} cells among gene sets associated with various T-cell subsets. **D,** Representative multicolor immunofluorescence image of CD4^{+} (red), GZMA^{+} (green), CD28^{low} (purple) T cells in an IgG_4-RD lesion. **E,** Relative proportions of CD28^{high} and ^{low} CD4^{+}CTLs in submandibular lesions of individual patients with IgG_4-RD (n = 6). *DAPI*, 4′-6-Diamidino-2-phenylindole, dihydrochloride.

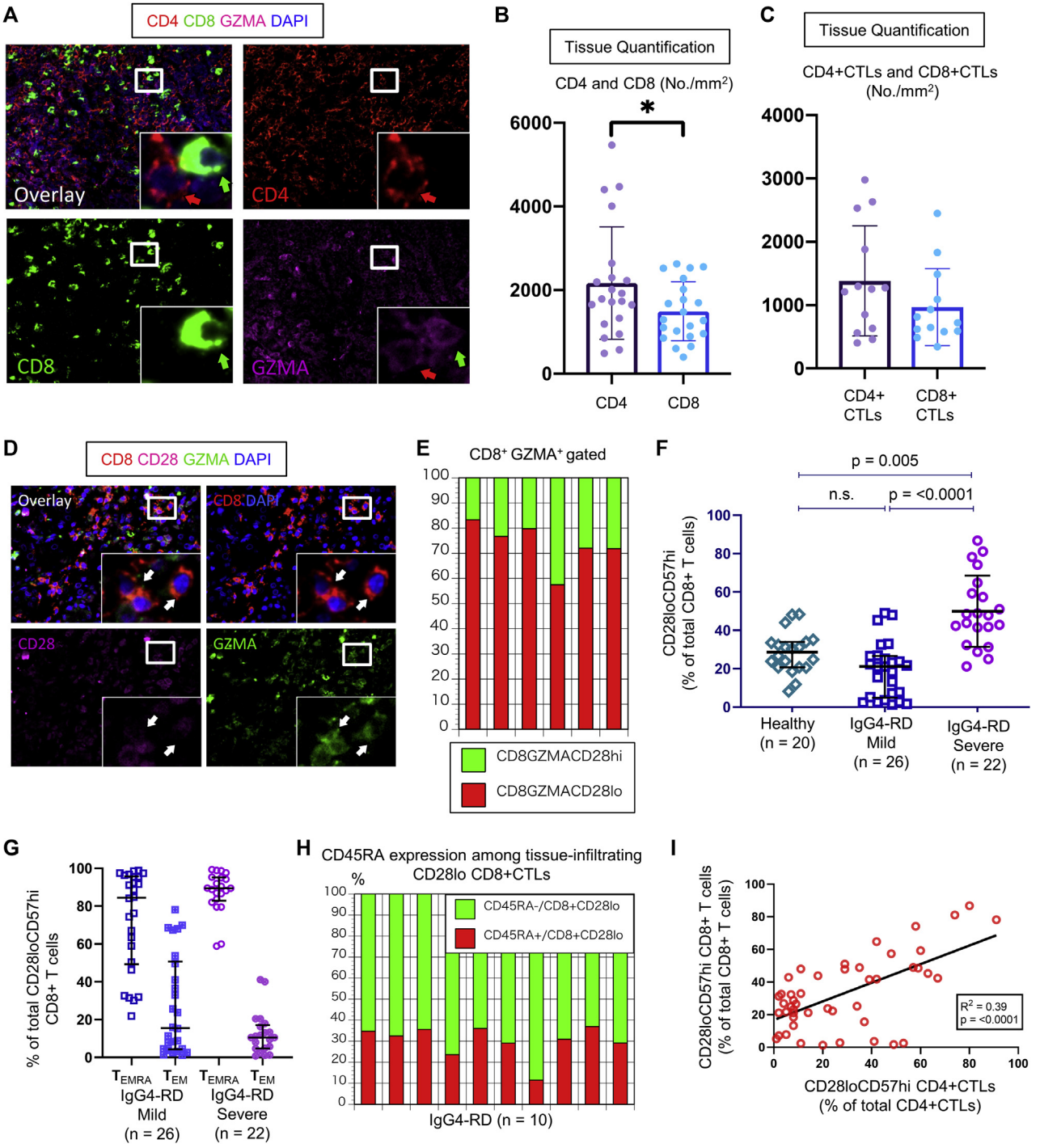

FIG 4. Effector $CD8^+$CTLs accumulate in the tissues and blood of patients with IgG_4-RD. **A,** Immunofluorescence image showing CD4 (red), CD8 (green), and GZMA (purple) staining in an IgG_4-RD lesion. Red arrows indicate $CD4^+$ $GZMA^+$ T cell. Green arrows indicate $CD8^+$ $GZMA^+$ T cell. **B,** Absolute number of $CD4^+$ T cells and $CD8^+$ T cells in tissues affected by IgG_4-RD (n = 21). **C,** Absolute number of $CD4^+$CTLs and $CD8^+$CTLs in tissues affected by IgG_4-RD (n = 13). **D,** Representative multicolor immunofluorescence image of CD8 (red), CD28 (purple), and GZMA (green) in an IgG_4-RD lesion. White arrows indicate $CD8^+$ $GZMA^+$ $CD28^{low}$ T cells. **E,** Relative proportions of $CD28^{hi}$ and $CD28^{lo}$ $CD8^+$ $GZMA^+$ T cells in tissues affected by IgG_4-RD (n = 6). **F,** Dot plot of flow cytometry data displaying significant accumulation of $CD28^{lo}CD57^{hi}$ $CD8^+$ T_{EM} cells in the blood of patients with IgG_4-RD (n = 48) compared with age-matched healthy donors (n = 20). Bars represent medians and interquartile ranges. *P* values calculated by ANOVA, with Kruskal-Wallis test to control for multiple comparisons. **G,** Dot plot of flow cytometry data showing that most $CD28^{lo}$ $CD57^{hi}$ $CD8^+$ T_{EM} cells in the blood of patients with IgG_4-RD accumulate in the T_{EMRA}, which is more pronounced in those with more severe disease. Bars represent medians and interquartile ranges. *P* values calculated by Mann-Whitney *U* test. **H,** Stacked bar chart showing that most $CD28^{lo}$ $CD8^+$ T cells infiltrating IgG_4-RD tissues have lost CD45RA expression, in contrast to their circulating counterparts presented in Fig 4, *G*. **I,** Scatter plot displaying the positive correlation between $CD28^{lo}CD57^{hi}$ $CD8^+$ T cells and $CD28^{lo}CD57^{hi}$ $CD4^+$CTLs in the blood of patients with IgG_4-RD. *P* value calculated by linear regression. *DAPI*, 4′-6-Diamidino-2-phenylindole, dihydrochloride; *n.s.*, nonsignificant.

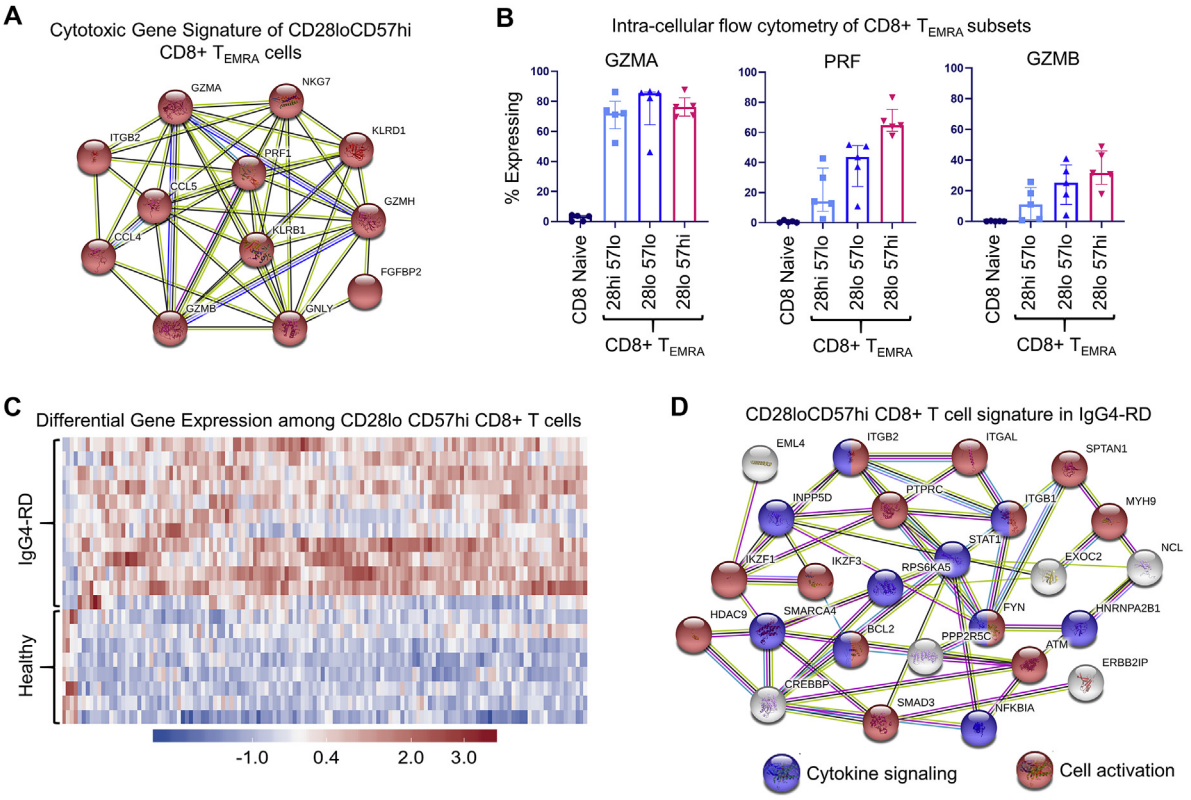

FIG 5. $CD28^{lo}$ $CD57^{hi}$ $CD8^{+}$ T cells display gene signatures of cytotoxicity, activation, and metabolism. **A,** STRING analysis representing predicted protein-protein interactions among upregulated genes by $CD28^{lo}CD57^{hi}$ $CD8^{+}$ T cells shows a cytotoxic gene signature. Number of lines connecting each node represents the degree of evidence for interaction. **B,** Intracellular flow cytometry for GZMA, PRF, and GZMB showing the greatest frequency of cytotoxic protein expression among $CD28^{lo}CD57^{hi}$ $CD8^{+}$ T_{EMRA} cells compared with other $CD8^{+}$ T_{EMRA}-cell subsets. Displayed are medians (bars) and interquartile range (error bars). **C,** Heatmap displaying 132 genes differentially expressed among $CD28^{lo}CD57^{hi}$ $CD8^{+}$ T cells from subjects with IgG_4-RD compared with those from healthy donors. **D,** STRING analysis representing predicted protein-protein interactions among upregulated genes by $CD28^{lo}CD57^{hi}$ $CD8^{+}$ T cells from subjects with IgG_4-RD compared with healthy donors showing signatures of cytokine signaling and activation. **E,** Dot plot displaying gene-set enrichment among $CD28^{lo}CD57^{hi}$ $CD8^{+}$ T cells from subjects with IgG_4-RD compared with those from healthy donors. *NFKB*, Nuclear factor kappa B; *STAT*, signal transducer and activator of transcription; *UV*, ultraviolet.

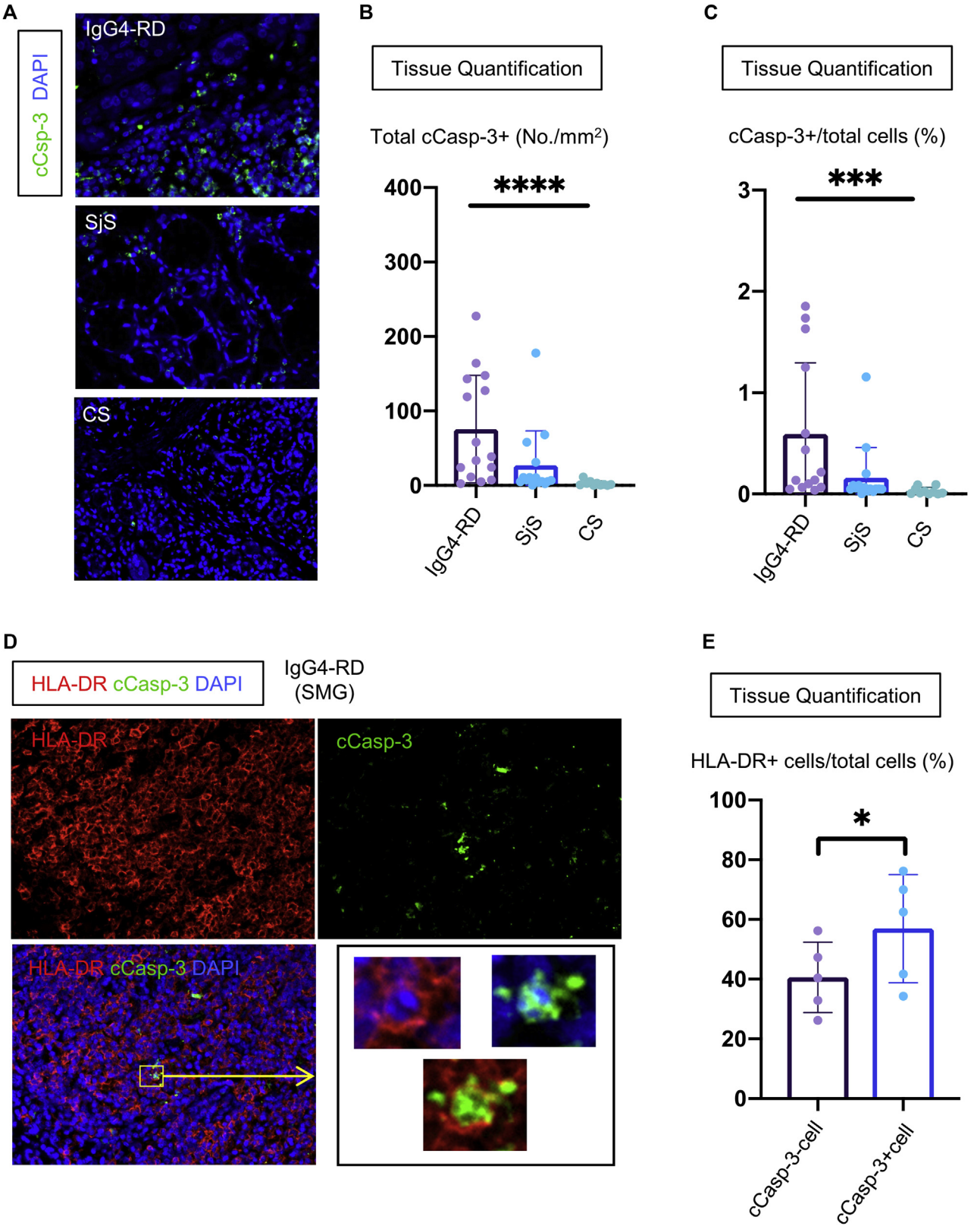

FIG 6. CD4^{+}CTLs and apoptotic cells expressing HLA-DR are abundant in tissues from patients with IgG$_4$-RD. **A,** Representative multicolor immunofluorescence images showing cleaved caspase-3 (cCasp-3) staining (green) in IgG$_4$-RD, Sjogren syndrome (SjS), and chronic sialadenitis (CS). **B** and **C,** Absolute numbers (Fig 6, *B*) and proportions (Fig 6, *C*) of cCasp-3 positive apoptotic cells in IgG$_4$-RD (n = 15), SjS (n = 15), and CS (n = 10). **D,** Representative multicolor immunofluorescence image of HLA-DR+ (red) cCasp-3+ (green) cells in an IgG$_4$-RD lesion. **E,** Percentages of HLA-DR^{+} cells in cCasp-3$^{+/-}$ cells in IgG$_4$-RD (n = 5). *DAPI*, 4′-6-Diamidino-2-phenylindole, dihydrochloride. Mann-Whitney *U* test used to calculate *P* value. Multiple comparisons controlled for by Kruskal-Wallis test. Error bars represent mean ± SEM. **P* < .05; ****P* < .001; *****P* < .0001.

or age-matched healthy donors, suggesting that these cells might be of pathogenic relevance (Fig 4, *F*). In addition, we found a proportional decline in $CD8^+$ naive T cells and increased $CD8^+$ T effector/memory RA-expressing (T_{EMRA}) cells in the blood of patients with IgG_4-RD with a more severe clinical phenotype (see Fig E8, *A-C*, in this article's Online Repository at www.jacionline.org).

Terminally differentiated $CD8^+$CTLs, defined as T_{EM} cells that have regained surface expression of CD45RA (T_{EMRA}), are reported to have enhanced cytotoxic capacity with increased perforin expression.[36] Among the $CD28^{lo}CD57^{hi}$ $CD8^+$CTLs observed in the blood of patients with IgG_4-RD, most of these cells were of the T_{EMRA} phenotype and this skewing was more pronounced in those with severe disease involvement (Fig 4, *G*). The gain of CD45RA expression by $CD8^+$ T_{EM} cells has been reported to be a reversible process, with the ability of $CD8^+$ T_{EMRA} cells to downregulate CD45RA expression following repeat antigen exposure.[37] Consistent with this possibility, we found that most infiltrating $CD28^{lo}$ $CD8^+$ T cells did not express CD45RA (Fig 4, *H*; see Fig E9 in this article's Online Repository at www.jacionline.org). In addition to tracking with disease severity, we found that circulating $CD28^{lo}CD57^{hi}$ $CD8^+$CTLs correlate strongly with circulating effector $CD4^+$CTLs and serum IgG_4 levels, 2 other surrogate markers related to disease severity (Fig 4, *I*; see Fig E10 in this article's Online Repository at www.jacionline.org).

To molecularly characterize $CD8^+$ T-cell subsets in the context of IgG_4-RD, we purified $CD8^+$ naive T cells, $CD28^{lo}CD57^{hi}$ $CD8^+$ T_{EM} cells, and $CD28^{lo}CD57^{hi}$ $CD8^+$ T_{EMRA} cells from the blood of patients with active IgG_4-RD and age-matched healthy donors. In contrast to the widely diverse TCR repertoire among $CD8^+$ naive T cells, we found that both the T_{EMRA} and T_{EM} $CD28^{lo}CD57^{hi}$ $CD8^+$ T cells were highly clonally expanded (in IgG_4-RD and healthy subjects alike) often with 1 or 2 clones dominating the TCR repertoire (see Fig E11 in this article's Online Repository at www.jacionline.org). The TCRβ gene usage was highly consistent between the $CD8^+$ T_{EM} and T_{EMRA} compartments within each individual subject, and the dominant clones were identical on the basis of CDR3 sequence between these compartments (Fig E11). The latter observation is consistent with the reversible gain and loss of CD45RA expression and dynamic exchange between the circulating $CD8^+$ T_{EM} and T_{EMRA} compartments. We also observed overlapping TCR Vβ gene usage across different patients with IgG_4-RD consisting of Vβ genes that were notably underrepresented among healthy donors, suggesting unique HLA class I-antigenic peptide recognition by $CD8^+$ T cells in IgG_4-RD that is shared across diseased individuals (Fig E11).

Finally, we performed RNA sequencing on the same purified $CD8^+$ T-cell subsets. We compared the transcriptional profiles from both T_{EMRA} and T_{EM} $CD28^{lo}CD57^{hi}$ $CD8^+$ cells from the blood of 5 patients with IgG_4-RD with those from 4 age-matched healthy donors. As expected, we observed a distinct gene signature of cytotoxicity among $CD28^{lo}CD57^{hi}$ $CD8^+$ T_{EMRA} cells (Fig 5, *A*). The cytotoxic transcriptional profile was similar to that observed within effector $CD4^+$CTLs with upregulation of genes such as *GZMA*, *GZMB*, *GZMH*, *GNLY*, *PRF1*, and *NKG7*. A heatmap and comprehensive list of differentially expressed genes between $CD8^+$ T_{EMRA} and $CD8^+$ naive T cells are provided in Figs E12 and E13 in this article's Online Repository at www.jacionline.org. An enhanced cytotoxicity profile among $CD28^{lo}CD57^{hi}$ $CD8^+$ T_{EMRA} cells was confirmed at the protein level by intracellular flow cytometry. These studies showed a high frequency of GZMA expression among all $CD8^+$ T_{EMRA} cell subsets, in contrast to the low frequency among naive $CD8^+$ T cells, as well as a gradation of both PRF and GZMB expression, with the greatest frequency being among $CD28^{lo}CD57^{hi}$ $CD8^+$ T_{EMRA} cells (Fig 5, *B*). These data parallel the findings of cytotoxicity presented above regarding $CD4^+$CTL subsets.

By comparing the transcriptome of $CD28^{lo}CD57^{hi}$ $CD8^+$CTLs from patients with IgG_4-RD with those from healthy donors, we identified 132 differentially expressed genes, the vast majority being upregulated (Fig 5, *C*). A full list of differentially expressed genes is available in Fig E14 in this article's Online Repository at www.jacionline.org. By mapping potential protein-protein interactions, we observed gene networks relevant to lymphocyte activation (FDR, 4.35×10^{-5}) and cellular response to cytokine signaling (FDR, 0.0216) (Fig 5, *D*) among cells from patients with IgG_4-RD. Upregulated genes relevant to T-cell activation included *FYN*, *PTPRC*, *IKZF3*, *IKZF1*, *HDAC9*, *ITGB1*, *ITGB2*, and *ITGAL*, whereas those related to cytokine signaling included *STAT1*, *SMAD3*, *NFKBIA*, *ITGB1*, and *ITGB2*. Relevant to cell survival, we found upregulation of the *IKZF3* and *BCL2* genes, both with important roles in suppressing apoptosis. Consistent with the predicted protein-protein interactions, gene-set enrichment analysis showed enrichment for gene sets related to cellular responses to cytokines (IFN-α, IFN-γ, TNF-α, IL-6/JAK/STAT3) and cell survival (apoptosis, p53 pathway, mitotic spindle, IL-2/STAT5) (Fig 5, *E*).

Apoptotic cells accumulate in tissues affected by IgG_4-RD

Because cell death mediated by cytotoxic T cells has been implicated in the pathogenesis of IgG_4-RD[33] and because we had observed the accumulation of both activated, effector $CD4^+$CTLs and $CD8^+$CTLs in the tissues affected by this disease, we costained tissue sections to determine the frequency of cellular apoptosis. Despite the efficiency with which macrophages clear apoptosing cells from inflamed tissues,[38] we observed a profoundly increased frequency of apoptotic cells in the tissues of patients with IgG_4-RD, representing as much as 2% of all nucleated cells (Fig 6, *A-C*). This frequency was significantly greater than that observed in noninflammatory controls as well as in salivary glands affected by Sjogren syndrome, a disease already linked to heightened apoptosis.[39] Consistent with a role for HLA class II–restricted $CD4^+$CTL-mediated apoptosis, we observed the preferential upregulation of HLA-DR in cells undergoing apoptosis (Fig 6, *F* and *G*; see Fig E15, *A*, in this article's Online Repository at www.jacionline.org). Through a series of multicolor immunofluorescence studies, we determined that $CD3^+$ T cells and vimentin$^+$ cells of mesenchymal origin account for most cells undergoing apoptosis (Fig 7; see Figs E15 and E16 in this article's Online Repository at www.jacionline.org). Given the clonal expansion and infiltration of effector T cells in these tissues, we expected to observe some activation-induced cell death of T cells. In stark contrast to our previous studies in systemic sclerosis, in which $CD31^+$ endothelial cells were the dominant target of apoptotic cell death,[21] and published reports on Sjogren syndrome, in which the preferential apoptosis of epithelial cells has been reported,[40] both of these specific cell

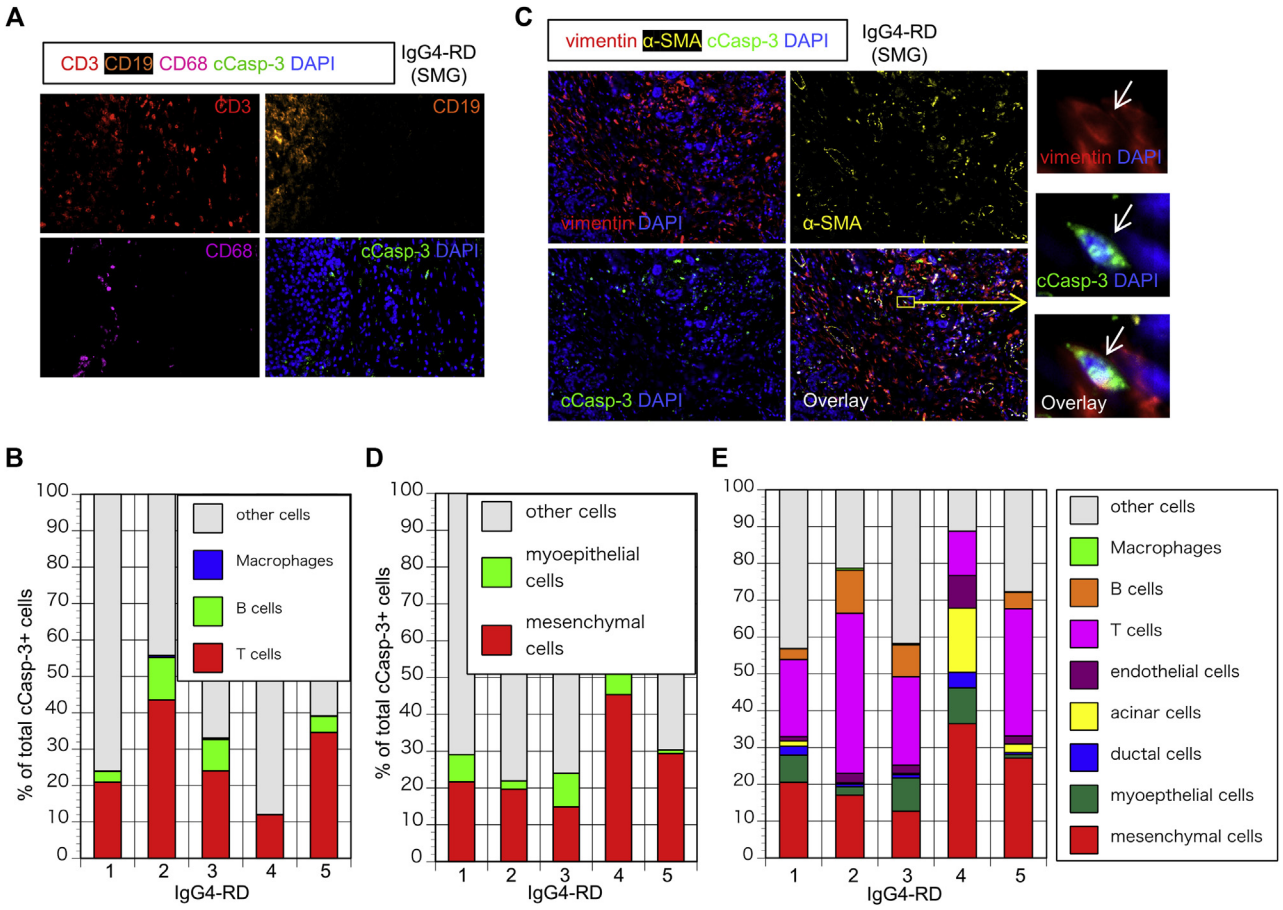

FIG 7. $CD3^+$ T cells and $vimentin^+$ cells account for a large proportion of apoptotic cells in tissues from patients with IgG_4-RD. **A,** Representative multicolor immunofluorescence image of CD3 (red), CD19 (orange), CD68 (purple), and $cCasp\text{-}3^+$ (green) staining in an IgG_4-RD lesion. White arrows indicate a $CD3^+$ $cCasp\text{-}3^+$ cell. **B,** Proportions of apoptotic cells in IgG_4-RD (n = 5) accounted for by T cells (red), B cells (green), macrophages (blue), and other cells (gray). **C,** Representative multicolor immunofluorescence images showing vimentin (red), α-SMA (yellow), and cCasp-3 (green) staining in an IgG_4-RD lesion. White arrows indicate a $vimentin^+$ $cCasp\text{-}3^+$ cell. **D,** Proportions of apoptotic cells in IgG_4-RD (n = 5) accounted for by mesenchymal cells (red) ($vimentin^+$, $\alpha\text{-}SMA^{+/-}$), myoepithelial cells (green) ($vimentin^-$, $\alpha\text{-}SMA^+$), and other cells (gray) ($vimentin^-$, $\alpha\text{-}SMA^-$). **E,** Relative proportions of each apoptotic cell type in each patient with IgG_4-RD (n = 5) are depicted. *DAPI*, 4′-6-Diamidino-2-phenylindole, dihydrochloride.

types infrequently underwent apoptosis in tissues affected by IgG_4-RD (Fig 7; Fig E16). To ask which cells in tissues undergo apoptotic death, we excluded apoptotic T cells from our analyses and thereby noted the preferential apoptosis of nonimmune, nonendothelial, $vimentin^+$ cells of mesenchymal origin in IgG_4-RD tissues (Fig 7, *E*).

DISCUSSION

The studies described here, taken in conjunction with our recent studies on another fibrotic disease, systemic sclerosis,[21] suggest a unifying model that may mechanistically unify clinically distinct autoimmune fibrotic disorders. Recurrent apoptotic death of specific disease-specific cell types, following the recognition of yet to be identified self-peptides by autoreactive $CD4^+$CTL and $CD8^+$CTL clones, may contribute to cell loss followed by an overly exuberant tissue remodeling process ending in fibrosis and organ dysfunction (Fig 8).

In this report, in-depth immunophenotyping studies were used to define distinct subsets of $CD4^+$CTLs in patients with IgG_4-RD. Specifically, we have defined $CD4^+$CTL subpopulations that are marked by the progressive loss of the surface costimulatory molecules CD27 and CD28, paired with the gain of expression of the glycoprotein CD57. We have demonstrated that the $CD27^{lo}CD28^{lo}CD57^{hi}$ $SLAMF7^+$ $CD4^+$ T-cell phenotype is highly enriched with features of cytotoxicity, and that this cell population has undergone marked clonal proliferation. This same $CD4^+$CTL subset expresses high levels of the chemokine receptor CX3CR1, consistent with previous reports in the context of the immune response to dengue virus.[30] The transcriptome of these $CD28^{lo}CD57^{hi}$ effector $CD4^+$CTLs suggests an activated phenotype with properties of tissue homing, orchestration of immune cell recruitment, TCR-mediated activation, and metabolic activity. Moreover, the clinical determinants of disease severity correlated with the degree of expansion of circulating effector $CD4^+$CTLs, suggesting their pathogenic role in the induction and/or progression of IgG_4-RD. Although we have quantified the direct tissue infiltration of $CD4^+$CTLs within IgG_4-RD lesions, the autoreactive nature of these cells and their contributions to pathogenesis have not yet been directly proven.

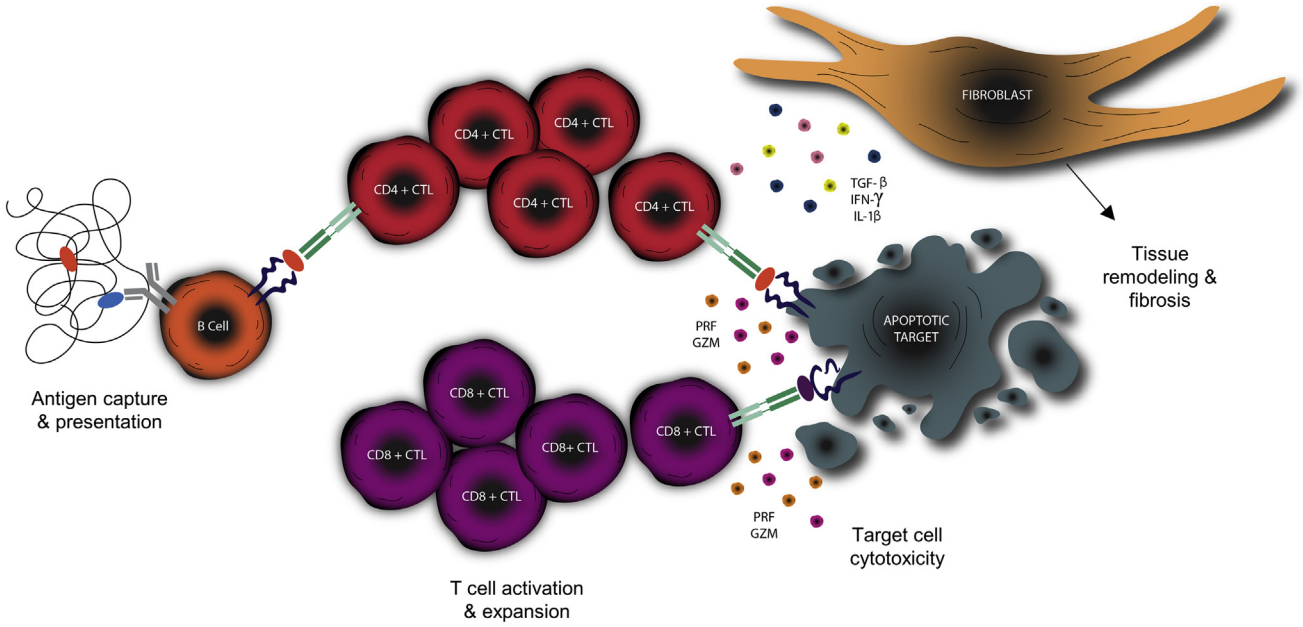

FIG 8. Schematic overview of proposed disease mechanism of IgG_4-RD. Activated B cells efficiently capture antigen and present peptide to $CD4^+$ T cells driving differentiation into a $CD4^+$CTL phenotype, activation, and clonal proliferation. Target cells upregulate HLA class II (in the appropriate inflammatory milieu) and act as antigen-presenting cells to expanded $CD4^+$CTLs, resulting in apoptotic cell death. Loss of antigen sequestration by apoptosing cells results in the cross-presentation by dendritic cells in the draining lymph node driving the activation and expansion of $CD8^+$CTLs. $CD8^+$CTLs travel to the site of inflammation and contribute to the cell death of apoptotic targets. Fibroblasts are activated by the secretion of profibrotic molecules by $CD4^+$CTLs, resulting in the production of extracellular matrix proteins to "fill the space" created by target-cell apoptosis.

In contrast to the pathogenic role of B cells in IgG_4-RD, which has been indirectly supported by their targeting of self-antigens[41] and more directly by the ameliorative effects of B-cell depletion with rituximab,[5] therapies specifically targeting T cells, or more precisely, $CD4^+$CTLs, have not been examined in this disease.

We have extended our previous finding that $CD4^+$CTLs dominate the tissue infiltrate in this disease by demonstrating that cytotoxic T cells in general are by far the most abundant T-cell type infiltrating tissues affected by IgG_4-RD, and that $CD4^+$CTLs and $CD8^+$CTLs contribute equally to the infiltrate. We have demonstrated abundant $GZMA^+$ $CD8^+$CTLs within lesional tissues with numbers that approximate those of infiltrating $CD4^+$CTLs and show that most tissue-infiltrating $CD8^+$CTLs have an activated phenotype. In the circulation, we describe a massive accumulation of $CD28^{lo}CD57^{hi}$ $CD8^+$ T cells in IgG_4-RD, most of which express cytotoxic markers and correlate tightly with disease severity and circulating effector $CD4^+$CTLs.

We also present the first evidence that enhanced apoptotic death, possibly driven by $CD4^+$CTLs and $CD8^+$CTLs, may be involved in the pathogenesis of IgG_4-RD. Although apoptosis has been reported in the settings of systemic sclerosis and Sjogren syndrome,[21,39,40,42] no such association has been previously documented in IgG_4-RD. Our quantitative finding of increased numbers of apoptotic cells within lesional tissues of IgG_4-RD is novel, and we additionally identify expression of HLA-DR on apoptotic cells suggesting the possibility of class II– restricted immune-mediated apoptosis in this disease. We also provide detailed tissue phenotyping to ascertain the origin of cells undergoing apoptosis. Excluding apoptotic T cells discussed below, nonendothelial, nonimmune $vimentin^+$ mesenchymal cells were the tissue cells most frequently undergoing apoptotic death. However, the final cellular identity of many apoptotic cells in IgG_4-RD remain to be determined. We identified very few apoptotic cells of endothelial origin in this disease, in stark contrast to our recent demonstration of predominant endothelial cell apoptosis in the context of systemic sclerosis.[21] The latter finding is potentially connected to the prominent vasculopathy observed in the clinical features of systemic sclerosis, which are notably lacking in the clinical manifestations of IgG_4-RD. The differences in cellular apoptosis between these 2 diseases suggests that breaks in immunologic tolerance to distinct self-antigens with differential expression across certain human cell types, presented by disease-specific HLA risk alleles, could in part explain the clinically distinct phenotypes of these 2 autoimmune fibrotic diseases.

Effector T cells go through the process of homeostatic contract by undergoing activation-induced cell death. Given the prominently activated phenotype of $CD4^+$ and $CD8^+$ T cells found in the blood and tissues of patients with IgG_4-RD, we consider it likely that much or all of the observed T-cell apoptosis is related to activation-induced cell death, which in some activated $CD4^+$ T cells is mediated by interactions between a Fas ligand and Fas/CD95.[43] Fas ligand was one of the upregulated transcripts in effector $CD4^+$CTLs (Fig 3, *C*). Alternatively, it is possible that some T cells present peptides on MHC class I molecules to autoreactive $CD8^+$CTLs and represent targets of cytotoxic cell death in this disease. Because activated T cells upregulate HLA class II molecules, it is formally possible that activated T cells may present endogenous peptides derived from lysosomal

degradation on HLA class II molecules to $CD4^+$CTLs. It is however very likely that most of the apoptotic $CD3^+$ T cells seen in IgG_4-RD tissues represent cells undergoing activation-induced cell death.

Precisely how $CD4^+$CTLs and $CD8^+$CTLs are linked in the pathogenesis of IgG_4-RD warrants further study. The presumed self-antigens that trigger both $CD4^+$ and $CD8^+$ T-cell clonal expansions in this disease remain to be identified. Although we observed a correlation between the circulating numbers of effector $CD4^+$CTLs and $CD8^+$CTLs, we envision a sequential process of immune responses initiated by distinct self-antigens normally located in different subcellular compartments to be the most likely mechanism by which the disease is initiated. Somatically mutated B cells likely most efficiently capture self-antigen(s) and present lysosomally derived peptides on HLA class II in disease lesions and repeatedly polarize activated $CD4^+$ T cells in tissue sites to assume a $CD4^+$CTL phenotype. Activated innate and adaptive immune cells secreting IFN-γ may induce HLA class II expression on mesenchymal cells. Activated $CD4^+$CTLs may induce apoptotic death of these mesenchymal cells and also secrete IL-1β and TGF-β, and thus assist in an overexuberant tissue repair process involving macrophages, fibroblasts, and myofibroblasts (Fig 8). The release of generally sequestered cytosolic or nuclear proteins from dying mesenchymal may result in a further break in tolerance, epitope spreading, and cross-presentation of these antigens by dendritic cells in the draining lymph node to activate self-reactive $CD8^+$ T cells. These cells then expand and are recruited to the sites of disease where they amplify the apoptotic death of target cells (Fig 8). Activation-induced cell death likely attenuates the expanded $CD4^+$CTL and $CD8^+$CTL clones in these lesions.

Tying the $CD8^+$CTL response observed in IgG_4-RD to the therapeutic efficacy of B-cell depletion also requires further consideration. The most likely scenario is the 2-step model described above, wherein B cells activate $CD4^+$CTLs that are the initiators of the disease and $CD8^+$CTLs are secondarily activated and contribute to an amplification process (Fig 8). We had previously reported that circulating $CD4^+$CTL numbers decline after B-cell depletion therapy in IgG_4-RD.[8] However, no evidence exists at present for $CD8^+$ T-cell attenuation after B-cell depletion and the *in vivo* relevance of the $CD8^+$ T-cell expansion to disease pathogenesis therefore remains unclear. We do observe a significant correlation between effector $CD8^+$CTL expansion in the blood and serum IgG_4 levels (Fig E10), providing a correlative suggestion that B-cell responses and $CD8^+$CTL expansion may be linked. The presentation of self-antigens by HLA class I molecules on B cells to $CD8^+$ T cells has been demonstrated in the context of autoimmune disease,[44] so a potential direct link between B cells and $CD8^+$ T cells in disease lesions might still be considered a possibility. We expect that the eventual identification of antigens recognized by clonally expanded $CD4^+$CTLs and $CD8^+$CTLs in IgG_4-RD will provide clarity regarding these possible mechanisms.

Conclusions

The studies presented here suggest that cytotoxic T cells from both $CD4^+$ and $CD8^+$ lineages may induce apoptotic cell death in IgG_4-RD lesions and that this potentially contributes to the pathogenesis of IgG_4-RD. These findings may have broad implications for the mechanisms that underlie immune-mediated fibrosis. The precise dissection of effector $CD4^+$CTL and $CD8^+$CTL subsets in the context of IgG_4-RD will facilitate subsequent work in the discovery of relevant cognate self- or exogenous peptides driving the adaptive immune responses observed in IgG_4-RD. This work further expands on the possibility that recurrent immune-mediated apoptosis of cells within chronically inflamed tissues may act as a mechanism that generates fibrosis.

Clinical implication: T-cell–mediated apoptosis in disease lesions may contribute to the induction of fibrosis in IgG_4-RD. Effector $CD4^+$CTLs and $CD8^+$CTLs correlate with disease severity in IgG_4-RD.

REFERENCES

1. Kamisawa T, Zen Y, Pillai S, Stone JH. IgG4-related disease. Lancet 2015;385:1460-71.
2. Stone JH, Zen Y, Deshpande V. IgG4-related disease. N Engl J Med 2012;366:539-51.
3. Wallace ZS, Naden RP, Chari S, Choi HK, Della-Torre E, Dicaire J-F, et al. The 2019 American College of Rheumatology/European League Against Rheumatism classification criteria for IgG_4-related disease. Ann Rheum Dis 2020;79:77-87.
4. Deshpande V, Zen Y, Chan JK, Yi EE, Sato Y, Yoshino T, et al. Consensus statement on the pathology of IgG4-related disease. Mod Pathol 2012;25:1181-92.
5. Carruthers MN, Topazian MD, Khosroshahi A, Witzig TE, Wallace ZS, Hart PA, et al. Rituximab for IgG4-related disease: a prospective, open-label trial. Ann Rheum Dis 2015;74:1171-7.
6. Della-Torre E, Rigamonti E, Perugino C, Baghai-Sain S, Sun N, Kaneko N, et al. B lymphocytes directly contribute to tissue fibrosis in patients with IgG4-related disease. J Allergy Clin Immunol 2020;145:968-81.e14.
7. Mahajan VS, Mattoo H, Deshpande V, Pillai SS, Stone JH. IgG4-related disease. Annu Rev Pathol 2014;9:315-47.
8. Mattoo H, Mahajan VS, Maehara T, Deshpande V, Della-Torre E, Wallace ZS, et al. Clonal expansion of CD4+ cytotoxic T lymphocytes in patients with IgG4-related disease. J Allergy Clin Immunol 2016;138:825-38.
9. Maehara T, Mattoo H, Ohta M, Mahajan VS, Moriyama M, Yamauchi M, et al. Lesional CD4+ IFN-γ+ cytotoxic T lymphocytes in IgG4-related dacryoadenitis and sialoadenitis. Ann Rheum Dis 2017;76:377-85.
10. Della-Torre E, Bozzalla-Cassione E, Sciorati C, Ruggiero E, Lanzillotta M, Bonfiglio S, et al. A CD8α- subset of CD4+SLAMF7+ cytotoxic T cells is expanded in patients with IgG4-related disease and decreases following glucocorticoid treatment. Arthritis Rheumatol 2018;70:1133-43.
11. Patil VS, Madrigal A, Schmiedel BJ, Clarke J, O'Rourke P, de Silva AD, et al. Precursors of human CD4+ cytotoxic T lymphocytes identified by single-cell transcriptome analysis [published online ahead of print January 19, 2018]. Sci Immunol. https://doi.org/10.1126/sciimmunol.aan8664.
12. Caielli S, Veiga DT, Balasubramanian P, Athale S, Domic B, Murat E, et al. A CD4+ T cell population expanded in lupus blood provides B cell help through interleukin-10 and succinate. Nat Med 2019;25:75-81.
13. Schmidt D, Goronzy JJ, Weyand CM. CD4+ CD7− CD28− T cells are expanded in rheumatoid arthritis and are characterized by autoreactivity. J Clin Invest 1996;97:2027-37.
14. Thewissen M, Somers V, Hellings N, Fraussen J, Damoiseaux J, Stinissen P. CD4+CD28null T cells in autoimmune disease: pathogenic features and decreased susceptibility to immunoregulation. J Immunol 2007;179:6514-23.
15. Sun Z, Zhong W, Lu X, Shi B, Zhu Y, Chen L, et al. Association of Graves' disease and prevalence of circulating IFN-gamma-producing CD28(−) T cells. J Clin Immunol 2008;28:464-72.
16. Fasth AER, Dastmalchi M, Rahbar A, Salomonsson S, Pandya JM, Lindroos E, et al. T cell infiltrates in the muscles of patients with dermatomyositis and polymyositis are dominated by CD28null T cells. J Immunol 2009;183:4792-9.
17. Gilani SR, Vuga LJ, Lindell KO, Gibson KF, Xue J, Kaminski N, et al. CD28 down-regulation on circulating CD4 T-cells is associated with poor prognoses of patients with idiopathic pulmonary fibrosis. PLoS One 2010;5:e8959.
18. Tabeya T, Yamamoto M, Naishiro Y, Ishigami K, Shimizu Y, Yajima H, et al. The role of cytotoxic T cells in IgG4-related dacryoadenitis and sialadenitis, the so-called Mikulicz's disease. Mod Rheumatol 2014;24:953-60.
19. Uhal BD. Apoptosis in lung fibrosis and repair. Chest 2002;122, 293S-8.
20. Jun J-B, Kuechle M, Harlan JM, Elkon KB. Fibroblast and endothelial apoptosis in systemic sclerosis. Curr Opin Rheumatol 2003;15:756-60.

21. Maehara T, Kaneko N, Perugino CA, Mattoo H, Kers J, Allard-Chamard H, et al. Cytotoxic CD4+ T lymphocytes may induce endothelial cell apoptosis in systemic sclerosis. J Clin Invest 2020;130:2451-64.
22. Wallace ZS, Khosroshahi A, Carruthers MD, Perugino CA, Choi H, Campochiaro C, et al. An international, multi-specialty validation study of the IgG4-related disease responder index. Arthritis Care Res (Hoboken) 2018;70:1671-8.
23. Heinle R, Chang C. Diagnostic criteria for sarcoidosis. Autoimmun Rev 2014;13: 383-7.
24. Vitali C, Bombardieri S, Jonsson R, Moutsopoulos HM, Alexander EL, Carsons SE, et al. Classification criteria for Sjögren's syndrome: a revised version of the European criteria proposed by the American-European Consensus Group. Ann Rheum Dis 2002;61:554-8.
25. Ecker RC, Steiner GE. Microscopy-based multicolor tissue cytometry at the single-cell level. Cytometry A 2004;59:182-90.
26. Parekh S, Ziegenhain C, Vieth B, Enard W, Hellmann I. zUMIs—A fast and flexible pipeline to process RNA sequencing data with UMIs. Gigascience 2018;7.
27. Trombetta JJ, Gennert D, Lu D, Satija R, Shalek AK, Regev A. Preparation of single-cell RNA-Seq libraries for next generation sequencing. Curr Protoc Mol Biol 2014;107:4.22.1-17.
28. Mamedov IZ, Britanova OV, Zvyagin IV, Turchaninova MA, Bolotin DA, Putintseva EV, et al. Preparing unbiased T-cell receptor and antibody cDNA libraries for the deep next generation sequencing profiling. Front Immunol 2013;4:456.
29. Newman AM, Liu CL, Green MR, Gentles AJ, Feng W, Xu Y, et al. Robust enumeration of cell subsets from tissue expression profiles. Nat Methods 2015;12:453-7.
30. Weiskopf D, Bangs DJ, Sidney J, Kolla RV, De Silva AD, de Silva AM, et al. Dengue virus infection elicits highly polarized CX3CR1+ cytotoxic CD4+ T cells associated with protective immunity. Proc Natl Acad Sci U S A 2015;112: E4256-63.
31. Tian Y, Babor M, Lane J, Schulten V, Patil VS, Seumois G, et al. Unique phenotypes and clonal expansions of human CD4 effector memory T cells re-expressing CD45RA. Nat Commun 2017;8:1473.
32. Fonseka CY, Rao DA, Teslovich NC, Korsunsky I, Hannes SK, Slowikowski K, et al. Mixed-effects association of single cells identifies an expanded effector CD4+ T cell subset in rheumatoid arthritis. Sci Transl Med 2018;10.
33. Sasaki T, Yajima T, Shimaoka T, Ogawa S, Saito T, Yamaoka K, et al. Synergistic effect of IgG4 antibody and CTLs causes tissue inflammation in IgG4-related disease. Int Immunol 2020;32:163-74.
34. Chattopadhyay PK, Betts MR, Price DA, Gostick E, Horton H, Roederer M, et al. The cytolytic enzymes granyzme A, granzyme B, and perforin: expression patterns, cell distribution, and their relationship to cell maturity and bright CD57 expression. J Leukoc Biol 2009;85:88-97.
35. Strioga M, Pasukoniene V, Characiejus D. CD8+ CD28− and CD8+ CD57+ T cells and their role in health and disease. Immunology 2011;134:17-32.
36. Sallusto F, Lenig D, Förster R, Lipp M, Lanzavecchia A. Two subsets of memory T lymphocytes with distinct homing potentials and effector functions. Nature 1999; 401:708-12.
37. Carrasco J, Godelaine D, Van Pel A, Boon T, van der Bruggen P. CD45RA on human CD8 T cells is sensitive to the time elapsed since the last antigenic stimulation. Blood 2006;108:2897-905.
38. Elliott MR, Koster KM, Murphy PS. Efferocytosis signaling in the regulation of macrophage inflammatory responses. J Immunol 2017;198:1387-94.
39. Nakamura H, Horai Y, Shimizu T, Kawakami A. Modulation of apoptosis by cytotoxic mediators and cell-survival molecules in Sjögren's syndrome. Int J Mol Sci 2018;19.
40. Masago R, Aiba-Masago S, Talal N, Zuluaga FJ, Al-Hashimi I, Moody M, et al. Elevated proapoptotic Bax and caspase 3 activation in the NOD.scid model of Sjögren's syndrome. Arthritis Rheum 2001;44:693-702.
41. Perugino CA, AlSalem SB, Mattoo H, Della-Torre E, Mahajan V, Ganesh G, et al. Identification of galectin-3 as an autoantigen in patients with IgG4-related disease. J Allergy Clin Immunol 2019;143:736-45.e6.
42. Sgonc R, Gruschwitz MS, Dietrich H, Recheis H, Gershwin ME, Wick G. Endothelial cell apoptosis is a primary pathogenetic event underlying skin lesions in avian and human scleroderma. J Clin Invest 1996;98:785-92.
43. Green DR, Droin N, Pinkoski M. Activation-induced cell death in T cells. Immunol Rev 2003;193:70-81.
44. Winer DA, Winer S, Shen L, Wadia PP, Yantha J, Paltser G, et al. B cells promote insulin resistance through modulation of T cells and production of pathogenic IgG antibodies. Nat Med 2011;17:610-7.